IOP Publishing New J. Phys. 27 (2025) 023037 https://doi.org/10.1088/1367-2630/adb779

New Journal of Physics
The open access journal at the forefront of physics

Deutsche Physikalische Gesellschaft DPG
IOP Institute of Physics

Published in partnership with: Deutsche Physikalische Gesellschaft and the Institute of Physics

OPEN ACCESS

RECEIVED
18 October 2024

REVISED
28 January 2025

ACCEPTED FOR PUBLICATION
18 February 2025

PUBLISHED
27 February 2025

PAPER

Proximity-induced anomalous topological superconductivity in an antiferromagnetic honeycomb-lattice

Fenghua Qi[1,*], **Yuanyuan Xiang**[2], **Jie Cao**[2] and **Guojun Jin**[3,4,*]

[1] School of Electronic Engineering, Nanjing Xiaozhuang University, Nanjing 211171, People's Republic of China
[2] College of Mechanics and Engineering Science, Hohai University, Nanjing 210098, People's Republic of China
[3] National Laboratory of Solid State Microstructures, Department of Physics, and Collaborative Innovation Center of Advanced Microstructures, Nanjing University, Nanjing 210093, People's Republic of China
[4] School of Physics Science and Technology, Kunming University, Kunming 650214, People's Republic of China
[*] Authors to whom any correspondence should be addressed.

E-mail: qifenghua.hi@163.com and gjin@nju.edu.cn

Keywords: anomalous topological superconductivity, proximity, antiferromagnetic honeycomb-lattice

Abstract

Topological superconductivity, generated in an engineered system with the proximity effect from an s-wave superconductor, usually requires the original sample to be a topological insulator. In this study, we propose a novel form of topological superconductivity in a honeycomb lattice arising from both antiferromagnetism (AFM) and s-wave superconductivity. Eventhough the honeycomb lattice with AFM is a normal insulator, the inherent topology of such a system is nontrivial. The topology of the system is determined by the relative values of the s-wave pairing potential and antiferromagnetic order. Notably, there are no chiral edge states at the open boundary if the engineered system is uniform everywhere, whether topologically trivial or not. However, when two parts with different topologies are brought together, two chiral edge states emerge at the topological phase boundary in the middle of the material. This challenges the bulk-edge correspondence observed in conventional topological materials. These chiral edge states are protected by valley symmetry and, owing to their Majorana fermion nature, can contribute to a half-integer quantized conductance.

1. Introduction

Topological superconductors (TSCs) are characterized by the presence of a superconducting gap in the bulk and Majorana fermions along their boundaries [1, 2]. These materials are highly sought after because Majorana fermions exhibit non-Abelian statistics, making them prime candidates for topological quantum computing [3–6]. Despite more than one decade of searching for TSCs [7–13], deterministic evidences for specific materials such as Sr_2RuO_4 [14] and UTe_2 [15] have yet to be established. The primary challenge lies in the fact that a comprehensive understanding of TSCs necessitates the inclusion of electron-electron interactions. Moreover, the Fermi surface and band topology of the normal state exert a significant influence on the outcomes. Consequently, it remains a prior unknown what the pairing and topology of the resulting superconducting ground state might be.

Another common approach involves an engineered system where an effective p-wave superconductor can be realized using a topological insulator (TI) in proximity contact with an s-wave superconductor [16–22]. Generally speaking, the s-wave superconductor is mostly regarded as a bulk metal at low temperatures. For example, Nb and NbN are promising materials. When graphene is brought into contact with Nb, an increase in the superconducting critical temperature is observed [23]. Hence, in figure 1, we use the shaded area to represent the region influenced by superconductivity without describing the structure of the s-wave superconductor. A crucial element in this system is the presence of spin–orbit coupling in TI, such as in the Kane–Mele model [24–28], extended Kitaev model [29–31], and Bernevig–Hughes–Zhang model [32–34], which can convert the s-wave pairing into an effective p-wave pairing in the resulting TSC. There exists a fundamental question about the necessity of a TI for engineering the TSC.

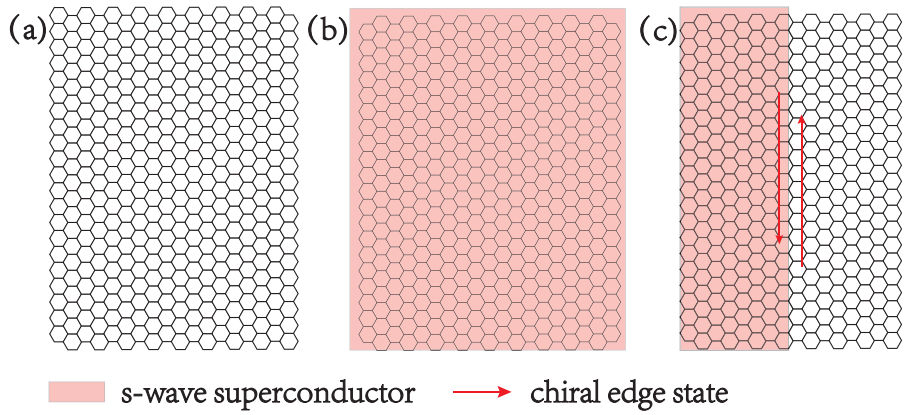

Figure 1. Illustration of three cases with boundary. The pure AFM honeycomb lattice (a) and wholly proximate to an s-wave superconductor with large pairing potential (b), there are no chiral edge states at the open boundary. However, when they are put together (c), there are two chiral edge states at the boundary within the bulk, indicating its topological characteristics.

A honeycomb lattice, known for its distinctive features of the Dirac dispersion and opposite Berry curvature around the two inequivalent valleys in the Brillouin zone, has become a paradigmatic system for exploring topological states. In this paper, we will broaden the previous investigations to incorporate antiferromagnetism (AFM) into the system, presenting a novel pathway to engineer topological superconductivity. Notably, TI is no longer needed in our approach while the non-zero Berry curvature and valley degree of freedom play the critical role. The AFM states on a honeycomb lattice have been well studied by the Kane–Mele-Hubbard model [35–38]. The enhancement of the Coulomb repulsion at half filling leads to phase transitions from a semimetal to an AFM Mott insulator. This condition can be achieved in a superatomic honeycomb lattice with each site occupied by a magnetic superatom [39]. The honeycomb lattice achieves perfect AFM alignment and it assumes that spin polarizations are opposite for different sublattices. Employing a mean-field treatment, we convert the AFM order into effective mass terms with opposite signs for different spins. For example, the spin-up electrons experience a positive mass term, while the spin-down electrons encounter a negative one. As a result, the Chern numbers of the conduction and valence bands in one valley become half-integers with different signs for different spins. Unlike the Kitaev honeycomb model [40], the AFM honeycomb system here is a normal insulator.

In the Bogoliubov–de Gennes (BdG) framework, the TSC here is treated at the mean-field level, and the BdG matrix of the TSC is formally equivalent to the Bloch matrix of TIs. When the Fermi level resides within the band gap, the break down of time-reversal ($\mathcal{T}$) symmetry by the AFM leads to the spin-up electron band and spin-down hole band below the Fermi level having the half-integer Chern numbers with the same signs in one valley. When summed over, the Chern number of the quasiparticle bands below the superconducting gap becomes a non-zero integer. Importantly, as the Chern number in the other valley has the same value but opposite sign, the honeycomb lattice manifests as a TSC with a total Chern number of zero but a non-zero valley Chern number. We name this new kind of TSC as a topological valley superconductor (TVSC).

One interesting thing is that, even though the TVSC is topological, there exist no chiral edge states at the boundary with vacuum. As shown in figure 1, the honeycomb lattice with the AFM order does not exhibit chiral edge states whether or not there is an s-wave superconductor wholly covered. However, if only half of the honeycomb lattice is covered with an s-wave superconductor featuring a pairing potential larger than the effective mass caused by the AFM, while the other half is still influenced by the AFM, at the boundary between these two regions, we observe two linear dispersions spanning the entire superconducting gap with opposite velocities. These are indeed two Majorana fermion dispersions originating from two valleys. Numerical calculations of the wave functions of these Majorana fermions confirm their localization near the region boundary. This peculiar phenomenon violates the bulk-edge correspondence in usual topological systems.

The remainder of this paper is structured as follows. In section 2, we briefly review the AFM honeycomb lattice model and the BdG equation. We analytically derive the non-zero valley Chern number. In section 3, we numerically calculate the band dispersion and chiral edge states in a ribbon structure with a topological phase boundary. Finally, we give a brief conclusion in section 4.

2. Model and formulation

2.1. The AFM honeycomb lattice model

We consider a monolayer honeycomb lattice taking into account the on-site Coulomb interaction. The system can be described by the Hubbard model as

$$H=\sum_{\langle i,j\rangle}-tc_i^{\dagger}\sigma_0 c_j+U\sum_i n_{i\uparrow}n_{i\downarrow}, \tag{1}$$

where the spinor operator $c_i^{\dagger}$ (c_i) creates (annihilates) an electron at site i, including two spins as its components. $\sum_i$ runs over all atomic sites and $\langle i,j\rangle$ denotes the summation over all pairs of nearest-neighboring sites for which the kinetic hopping parameter is t. σ_0 is the 2×2 identity matrix and $(\sigma_x,\sigma_y,\sigma_z)$ are the spin Pauli matrices used later. In the half-filling case with the mean-field approximation, the interaction term can be written as

$$U\sum_i n_{i\uparrow}n_{i\downarrow}\approx U\sum_i\left(n_{i\uparrow}\langle n_{i\downarrow}\rangle+\langle n_{i\uparrow}\rangle n_{i\downarrow}\right). \tag{2}$$

For a pristine honeycomb lattice at half-filling, the Coulomb interaction is known to induce a phase transition from the nonmagnetic state to the AFM state when $U>U_c$, with the order parameter $\langle S_i^z\rangle=\langle n_{i\uparrow}\rangle-\langle n_{i\downarrow}\rangle\neq 0$. In the half-filling case, the mean field approximation obtained that $U_c\sim 2.2t$ [41], while quantum Monte Carlo calculations indicate that $U_c\sim 4.5t$ [42]. In the AFM state, the Coulomb interaction could generate an electronic gap due to the breaking of inversion symmetry since the spin occupations on sublattices A and B are different. Meanwhile, the $\mathcal{T}$ symmetry is also broken by the AFM order that makes the TSC possible.

In this work, we are primarily interested in the behavior of the superconducting state, and assume that $\langle S_i^z\rangle$ is not notably affected by the superconductivity [43], we can safely use a fixed spin-related sublattice potential $M=(U/2)\langle S_{\rm A}^z\rangle=-(U/2)\langle S_{\rm B}^z\rangle$ to represent the AFM model as

$$H=\sum_i\Psi_i^{\dagger}\left(-t\sigma_0\tau_x+M\sigma_z\tau_z\right)\Psi_i, \tag{3}$$

where $\Psi_i=(c_{i\rm A},c_{i\rm B})^{\rm T}$ and τ is the sublattice index. The AFM model is similar to the inversion symmetry breaking Semenoff insulator [44] with the difference that the sublattice potential M changes sign for different spins. Previous study of the AFM model showed that the spin-polarized states arised at the domain wall will exhibit a circular dichroism Hall effect, since there are different AFM orders on both sides of the domain wall [45]. It is worth mentioning that both the Semenoff model and the AFM model are normal insulators using the Chen number for classification.

To better illustrate the Berry curvature features of the AFM model, equation (3) can be Fourier transformed into the momentum space and then rewritten as the low-energy Hamiltonian

$$H=\sum_{\boldsymbol{k}}\left(\Psi_{+\boldsymbol{k}}^{\dagger},\Psi_{-\boldsymbol{k}}^{\dagger}\right)\begin{pmatrix}h_+(\boldsymbol{k},\sigma_z) & 0\\ 0 & h_-(\boldsymbol{k},\sigma_z)\end{pmatrix}\begin{pmatrix}\Psi_{+\boldsymbol{k}}\\ \Psi_{-\boldsymbol{k}}\end{pmatrix}, \tag{4}$$

where $h_\eta(\boldsymbol{k},\sigma_z)=v_{\rm F}\sigma_0\left(\tau_x k_x+\eta\tau_y k_y\right)+M\sigma_z\tau_z$, $\eta=\pm$ is the valley index for the $\pm$K valleys, the Fermi velocity $v_{\rm F}=\sqrt{3}at/2$ and a is the lattice constant of the honeycomb lattice.

This Dirac Hamiltonian gives the analytical expression of the Berry curvature of the valence band in the vicinity of the Dirac points as [46, 47]

$$\Omega_\eta(\boldsymbol{k})=-\eta\sigma_z\frac{Mv_{\rm F}^2}{2\left(k^2v_{\rm F}^2+M^2\right)^{3/2}}. \tag{5}$$

As shown in figure 2, for a certain spin, the Berry curvatures change sign for the $+$K and $-$K valleys, so the Chern number of the valence band $C=\frac{1}{2\pi}\int\Omega(\boldsymbol{k})\mathrm{d}\boldsymbol{k}$ is zero as the Berry curvatures at the two valleys exactly cancel out each other while the Chern number of one spin-valley is $\pm 1/2$. On the other hand, due to the AFM, the Berry curvatures of different spins also cancel each other. Hence, the total Chern number of the valence band in one valley is also zero.

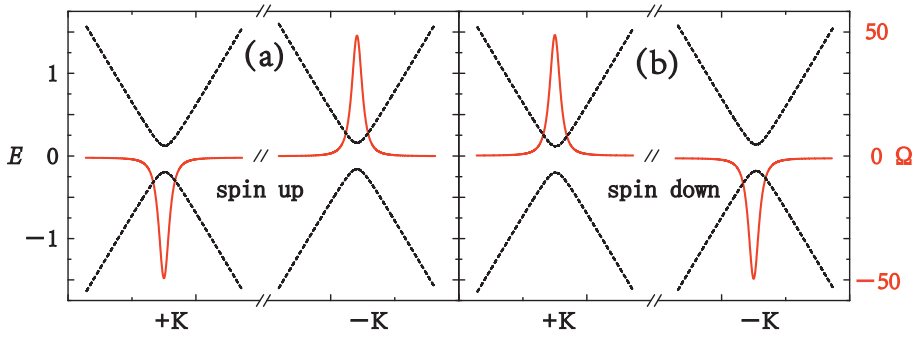

Figure 2. Band structures (black dashed lines) and Berry curvatures (red solid lines) of the AFM model in the vicinity of the Dirac points for different spins. (a) For the spin up band, the Berry curvatures are negative in the +K valley but positive in the −K valley, hence the total Berry phase vanishes. (b) For the spin down band, the Berry curvatures are negative in the −K valley but positive in the +K valley. For illustration only, we take $M = 0.1t$.

2.2. The BdG equation of TVSC

We further consider an AFM honeycomb lattice covered by an s-wave superconducting electrode. Electron and hole excitations are described by the BdG equation [48]

$$\begin{pmatrix} H-\mu & \Delta I_0 \\ \Delta I_0 & \mu - \mathcal{T}H\mathcal{T}^{-1} \end{pmatrix} \begin{pmatrix} u \\ v \end{pmatrix} = \varepsilon \begin{pmatrix} u \\ v \end{pmatrix}, \tag{6}$$

where I_0 is the 4×4 unitary matrix, u and v being the electron and hole wave functions, ε is the excitation energy (relative to the Fermi energy μ). Here we use the low energy Hamiltonian in equation (4) and take Δ to be real. The $\mathcal{T}$ operator interchanges the valleys and spins as

$$\mathcal{T} = \begin{pmatrix} 0 & \tau_z \\ \tau_z & 0 \end{pmatrix} i\sigma_y \mathcal{C}, \tag{7}$$

with $\mathcal{C}$ the operator of complex conjugation. Therefore, the BdG equation is decoupled into two sets in the form

$$\begin{pmatrix} h_\pm(\boldsymbol{k},\sigma_z)-\mu & \Delta I_0 \\ \Delta I_0 & \mu - h_\pm(\boldsymbol{k},-\sigma_z) \end{pmatrix} \begin{pmatrix} u_{\boldsymbol{k}} \\ v_{\boldsymbol{k}} \end{pmatrix} = \varepsilon_{\boldsymbol{k}} \begin{pmatrix} u_{\boldsymbol{k}} \\ v_{\boldsymbol{k}} \end{pmatrix}. \tag{8}$$

Consider the case $\eta = +$, where the electron part is contributed by the spin-up band in +K valley, and the hole part is contributed by the spin-down band in −K valley. When the Fermi energy lies within the electron band gap and Δ is small, the Chern number of the quasiparticle band below μ becomes -1 instead of 0. We can understand it from figure 2. The valence band of the spin-up electron part contributes $-1/2$ to the Chern number, while $\mathcal{T}$ changes the sign of the Berry curvature of the spin-down hole part, contributing another $-1/2$ to the Chern number. Therefore, the superconducting gap in the +K valley is not topologically trivial, even though it is an s-wave pairing gap. On the other hand, as the counterpart of the +K valley, the case in the −K valley is exactly opposite. The Chern number of the quasiparticle band below μ is 1 in the −K valley. Similar to the spin Hall insulator and valley Hall insulator, a topological invariant can be used to describe this nontrivial topology. The Chern numbers provided by the BdG bands (8) are $C_+ = -1$ and $C_- = 1$. It can be seen that the total Chern number of the superconductor system is $C_{\text{total}} = C_+ + C_- = 0$. However, the valley Chern number of this TSC can be defined as $C_{\text{VS}} = (C_+ - C_-)/2 = -1$. The non-zero C_{VS} indicates that this new type of the TSC is topologically nontrivial, and we refer to it as a TVSC.

3. Results and discussion

3.1. Topological phase transition

By setting $\mu = 0$, we can analytically derive the condition for topological phase transition. Taking the +K valley for instance, the BdG Hamiltonian is explicitly written as

$$H_{\text{BdG}}(\boldsymbol{k}) = \begin{pmatrix} v_{\text{F}}\boldsymbol{\tau}\cdot\boldsymbol{k} + M\tau_z & \Delta\tau_0 \\ \Delta\tau_0 & -v_{\text{F}}\boldsymbol{\tau}\cdot\boldsymbol{k} + M\tau_z \end{pmatrix}, \tag{9}$$

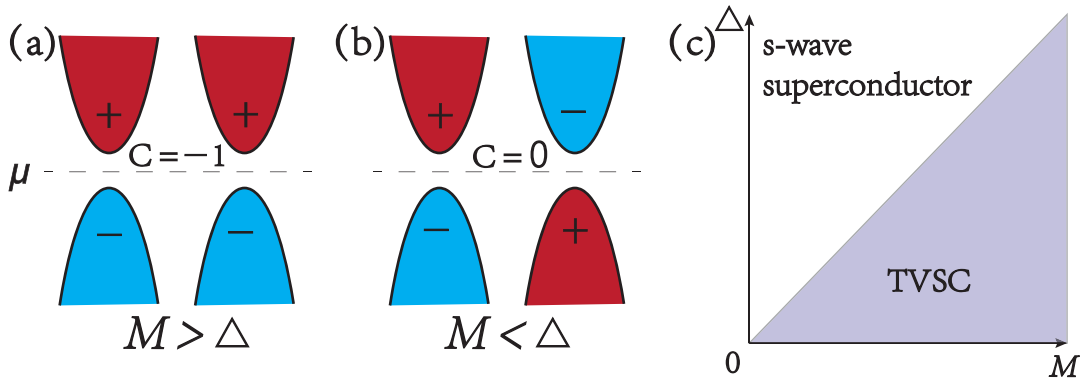

Figure 3. Schematic illustration of the band structures and Berry curvatures of the two sets of Dirac Hamiltonian in equation (12). (a) For $M > \Delta$, the Berry curvatures of the bands below μ have the same sign, resulting in a Chern number of -1. (b) For $M < \Delta$, the Berry curvatures of the bands below μ have opposite signs, resulting in a Chern number of 0. Here $\pm$ respectively represents $C = \pm\frac{1}{2}$. (c) Phase diagram with respect to the parameters M and Δ.

where $\boldsymbol{\tau} = (\tau_x, \tau_y)$ and the spin indices are neglected. Using the unitary transformation $H'_{\mathrm{BdG}} = \mathcal{U}^\dagger H_{\mathrm{BdG}} \mathcal{U}$ with $\mathcal{U} = \mathcal{U}_1 \mathcal{U}_2$, in which

$$\mathcal{U}_1 = \begin{pmatrix} \cos(\pi/4) & -\sin(\pi/4) \\ \sin(\pi/4) & \cos(\pi/4) \end{pmatrix} \bigotimes \tau_0, \tag{10}$$

and

$$\mathcal{U}_2 = \begin{pmatrix} 1 & 0 & 0 & 0 \\ 0 & 0 & 0 & 1 \\ 0 & 0 & 1 & 0 \\ 0 & 1 & 0 & 0 \end{pmatrix}, \tag{11}$$

the resultant BdG Hamiltonian is further decoupled as

$$H'_{\mathrm{BdG}} = \begin{pmatrix} v_{\mathrm{F}} \boldsymbol{\tau} \cdot \boldsymbol{k} + (\Delta + M)\tau_z & 0 \\ 0 & v_{\mathrm{F}} \boldsymbol{\tau} \cdot \boldsymbol{k} + (M - \Delta)\tau_z \end{pmatrix}. \tag{12}$$

The two decoupled sets correspond exactly to the massive Dirac Hamiltonian, and the sign of the Berry curvature is determined by the sign of the mass term. As illustrated in figure 3, it is evident that the topological phase transition occurs at $M = \Delta$. For $M > \Delta$, the system exhibits characteristics of a TVSC, while for $M < \Delta$, the system is a topologically trivial superconductor.

3.2. Novel edge states at the phase boundary

As a TSC, characterized by a seemingly simple heterostructure, i.e. a honeycomb lattice with the AFM ordering covered by an s-wave superconducting electrode, there have been less reported instances in the literature. The main reason may be that there are no edge states in the open boundary, which violates the bulk-edge correspondence seen in normal topological materials. In figure 4(a), we present a quasi-one-dimensional ribbon fully covered by an s-wave superconducting electrode with $M > \Delta$. The corresponding band structure reveals that the localized edge states, extending from the conduction band bottoms of the two valleys, do not cross the superconducting gap, despite our analysis indicating that the system is in a TVSC state.

As per equation (12), our analysis reveals that the system undergoes a topological phase transition when $M = \Delta$. The phase diagram is illustrated in figure 3(c). To explore this, we create a boundary in the middle of a honeycomb lattice nanoribbon, as depicted in figure 4(b), where the left half is covered by an s-wave superconducting electrode with $M < \Delta$, and the right half is uncovered. The resulting band structure displays two linear dispersions crossing the superconducting gap, indicating the nature of topological phase changing across the boundary.

This peculiar result can be well explained by combining with another intriguing observation. According to equation (12), our analysis indicates that the system is in a TVSC state even in the limit $\Delta \to 0$. This seems contradictory since, for $\Delta = 0$, there is no superconductivity, and hence no TVSC. This apparent paradox can be reconciled if we admit the fact that the edge states of the TVSC are absent at the open boundary with

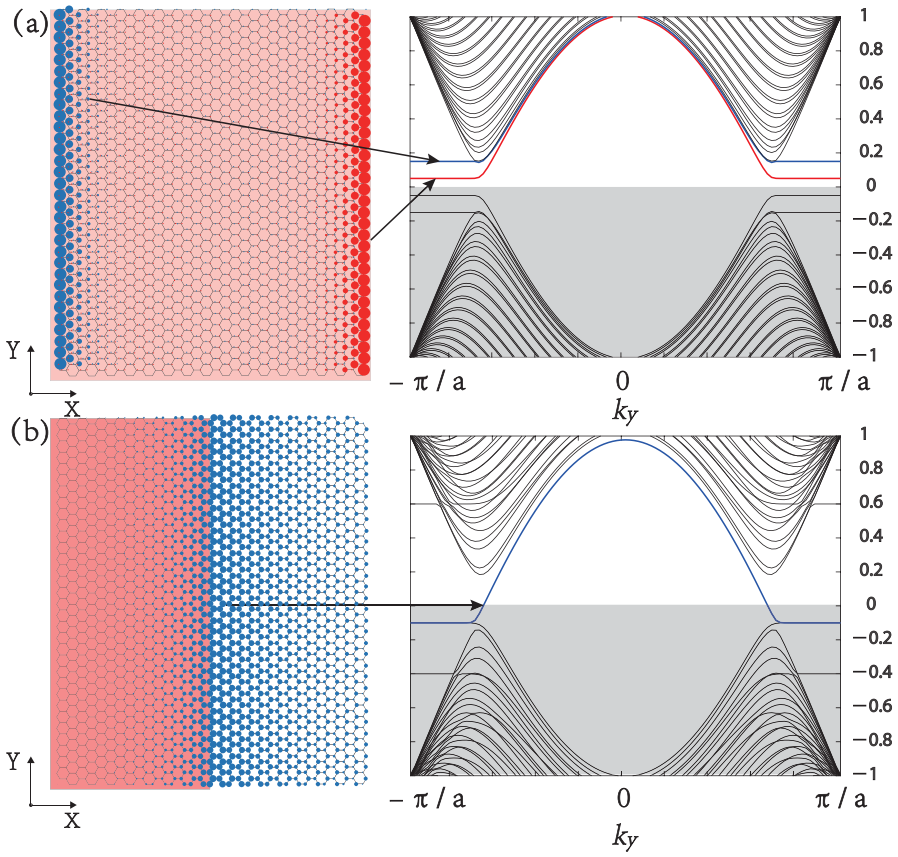

Figure 4. Real-space wave functions and band structures of a honeycomb nanoribbon with the AFM order and proximate to an s-wave superconductor. The pink shaded region represents the s-wave superconductor and the width of the nanoribbon is approximately 4 nm. The mean-field AFM order is set as $M = 0.1t$. (a) The nanoribbon is entirely covered by the superconductor with $\Delta = 0.05t$. The edge states, colored in red and blue, do not cross the superconducting gap, even though the system is in the TVSC state. (b) The left-half nanoribbon, which is covered by an s-wave superconductor with $\Delta = 0.5t$, is a topologically trivial superconductor. The right-half, on the other hand, is indeed in the TVSC state eventhough $\Delta = 0$. The chiral edge states occurs and exponentially decrease away from the boundary.

vacuum as shown in figure 4(a). Only in the special constructed phase boundary, as shown in figure 4(b) where the right half is seen as a TVSC state, the chiral edge states occurs. Analysis of the wave function confirms that these linear dispersions are localized near the boundary between the left topologically trivial superconductor region and the right TVSC region. Consequently, the bulk-edge correspondence remains valid at the boundary of the topological phase transition within the bulk material, though not at the boundary with the vacuum.

Hence, we have identified a novel type of TSC that challenges the conventional bulk-edge correspondence. Nevertheless, upon introducing a topological phase boundary within the AFM honeycomb lattice, chiral edge states emerge, localized near this boundary. We also consider the case where $\mu \neq 0$ and found the existence of chiral edge states as long as $|\mu| < M$, thereby confirming its topological nature. Outside this parameter range, the edge states become mixed with the bulk states in the area not covered by the superconductor.

3.3. Chiral Majorana fermions and half-integer conductance

Several proposals for realizing Majorana fermion state with conventional superconductivity have been investigated by making use of strong spin–orbit coupling [16, 49]. The chiral Majorana fermions originated from the TI chiral edge states proximate to an s-wave superconductor come in pairs, since the chiral electron edge states can be viewed as a superposition of two identical branches of chiral Majorana fermions. In such systems, the transport properties are exactly the same as in the TI case, unless one can eliminate one branch of chiral Majorana fermions using a magnetic field [34].

In our proposal, we can see that the two linear dispersion edge states cross the superconducting gap in figure 4(b), in fact they are chiral Majorana fermions protected by the valley symmetry. We numerically confirm that the wave functions of the electron part and hole part are exactly the same. Due to the fact that the Chern numbers of each valley are ± 1, there is only one branch of chiral Majorana fermions for each

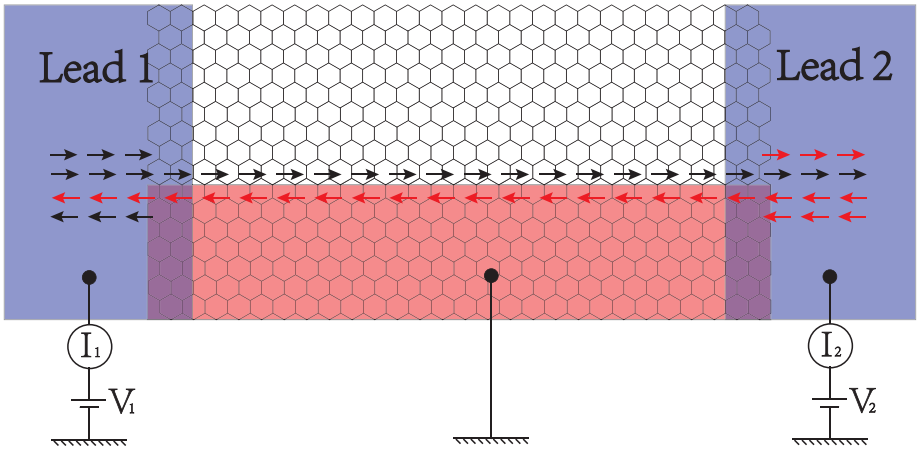

Figure 5. Schematic experimental setup for measuring conductivity. The black (red) arrows represents the Majorana fermions coming from lead 1 (2).

valley. Although the chiral Majorana fermions appear in pairs at the same phase boundary, they are from different valleys and drifting in different directions. During the transport measurement, the two branches of chiral Majorana fermions carry different voltage information from different leads and different valleys. Hence, one can measure a half-integer conductance plateau to verify the existence of the chiral Majorana fermions [10, 50].

The general relationships between current and voltage on leads 1 and 2 shown in figure 5 are $I_1 = (e^2/h)[(1 - R + R_A)V_1 - (T' - T'_A)V_2]$, and $I_2 = (e^2/h)[(1 - R' + R'_A)V_2 - (T - T_A)V_1]$. Here we set the voltage of the s-wave superconductor layer is 0, I_1 and I_2 are currents flowing into leads 1 and 2, respectively. R, T, R_A and T_A are the normal reflection, normal transmission, Andreev reflection and Andreev transmission probabilities for an electron injected from the left, while R', T', R'_A and T'_A are for an electron coming from the right. The two-terminal conductance is then defined as $\sigma_{12} = (I_1 - I_2)/2(V_1 - V_2)$ [50]. In the ideal case, i.e. $R = R_A = T = T_A = R' = R'_A = T' = T'_A = 1/4$, it is easy to obtain a half-integer quantized conductance $\sigma_{12} = e^2/2h$.

In figure 5, we illustrate the experimental setup of our proposal. In the ideal case, an electron coming from lead 1, for instance, is viewed as two right-going Majorana fermions. At the boundary between lead 1 and the central material, only one Majorana fermion is allowed to propagate through the chiral Majorana fermion channel in the middle region. The other Majorana fermion is backscattered into lead 1 and combines with the Majorana fermion transported from lead 2 to form a normal electron. A similar process occurs in lead 2. Therefore, during the transport, only half of an electron contributes to the conductivity, and the measured conductivity is a half-integer.

Even though the chiral Majorana fermions are protected by the valley symmetry, any perturbation (impurities, lattice defects like vacancies, for instance) that produces intervalley scattering will mix the two modes. It seems like that these perturbations will annihilate the Majorana modes, however, we can prove that regular scattering terms cannot destroy the chiral modes at the boundary. We start with a one-dimensional model to describe the low-energy chiral Majorana fermions. The Hamiltonian at the edge is $H_{\text{edge}} = \sum_k vk\gamma_{-k,+}\gamma_{k,+} - vk\gamma_{-k,-}\gamma_{k,-}$, where $\gamma_{k,\pm}$ are Majorana fermion operators satisfying $\gamma^\dagger_{k,\pm} = \gamma_{-k,\pm}$ and $\{\gamma_{-k,\eta}, \gamma_{k',\eta'}\} = \delta_{kk'}\delta\eta\eta'$. The k indices in both valleys are relative to the intersection of the edge state and the Fermi surface. It is worth noticing that if we combine two Majorana fermion operators into a complex fermion operator, $\phi_k = 1/\sqrt{2}(\gamma_{k,+} + i\gamma_{-k,-})$, the edge Hamiltonian can be written as $H_{\text{edge}} = \sum_k vk\phi^\dagger_k\phi_k$ [34]. Consider a regular intervalley scattering term which include two Majorana Fermions with the same energy, i.e. $H'_{\text{edge}} = \sum_k i\lambda\gamma_{-k,+}\gamma_{-k,-} - i\lambda\gamma_{k,-}\gamma_{k,+}$, where λ is constant represents the strength of the scattering. It is easy to prove that the Hamiltonian at the edge can be written as $H_{\text{edge}} + H'_{\text{edge}} = \sum_k (vk + \lambda)\phi^\dagger_k\phi_k$, up to a trivial shift of the energy. This is nothing but a shift of the origin of coordinates of k. We can then decompose the complex fermion operator into its real parts and obtain the same chiral Majorana fermion operators. Therefore, we conclude that the chiral Majorana fermions are well preserved in the presence of regular intervalley scattering terms.

4. Summary

In summary, the pursuit of TSCs has been fueled by the prospect of harnessing Majorana fermions for topological quantum computing. Despite more than one decade of efforts, a general synthesis method remains elusive, largely due to the intricate interplay of electron-electron interaction, Fermi surface characteristics, and band topology within the many-body interaction model. The use of engineered systems, particularly those incorporating TIs and the s-wave superconducting proximity effect, has provided an alternative avenue. Notably, the role of a TI in the engineered systems raises a question about its necessity.

The study here has explored the integration of the AFM into the honeycomb lattice, renowned for its unique Dirac dispersion and Berry curvature properties. The results have established a novel pathway to achieve the TSC without the requirement of a TI. The AFM arrangement, assuming opposite spin polarizations for different sublattices, has lead to the perfect alignment in the honeycomb lattice. Utilizing a mean-field treatment, the AFM has converted into effective mass terms, resulting in the half-integer Chern numbers for the conduction and valence bands in one valley with different signs for different spins. In the BdG framework, the TSC has been treated at the mean-field level, leading to the identification of a TVSC in the honeycomb lattice. Interestingly, the TVSC has exhibited a total Chern number of zero but a non-zero valley Chern number, despite the absence of chiral edge states at the lattice boundary with vacuum. Further investigation has revealed a unique phenomenon where, when only half of the honeycomb lattice is covered by an s-wave superconductor with a pairing potential exceeding the AFM-induced effective mass, two Majorana fermion dispersions have emerged at the boundary between the covered and uncovered regions. This violation of the bulk-edge correspondence in typical topological systems has highlighted the distinctive characteristics of the TVSC.

Data availability statement

All data that support the findings of this study are included within the article (and any supplementary files).

Acknowledgments

This work was supported by the National Natural Science Foundation of China (Grant Nos. 12104232, 12074156 and 22075068), the Fundamental Research Funds for the Central Universities (Grant No. B230201042) and STITP (Grant Nos. 202411460027Z and 202311460036Z).

ORCID iDs

Yuanyuan Xiang https://orcid.org/0000-0002-9218-1886
Guojun Jin https://orcid.org/0000-0001-8184-9249

References

[1] Qi X-L and Zhang S-C 2011 *Rev. Mod. Phys.* **83** 1057
[2] Sato M and Ando Y 2017 *Rep. Prog. Phys.* **80** 076501
[3] Ivanov D A 2001 *Phys. Rev. Lett.* **86** 268
[4] Kitaev A Y 2003 *Ann. Phys., NY* **303** 2
[5] Nayak C, Simon S H, Stern A, Freedman M and Das Sarma S 2008 *Rev. Mod. Phys.* **80** 1083
[6] Lian B, Sun X-Q, Vaezi A, Qi X-L and Zhang S-C 2018 *Proc. Natl Acad. Sci. USA* **115** 10938
[7] Mourik V, Zuo K, Frolov S M, Plissard S R, Bakkers E P A M and Kouwenhoven L P 2012 *Science* **336** 1003
[8] Nadj-Perge S, Drozdov I K, Li J, Chen H, Jeon S, Seo J, MacDonald A H, Bernevig B A and Yazdani A 2014 *Science* **346** 602
[9] Yin J-X *et al* 2015 *Nat. Phys.* **11** 543
[10] He Q L *et al* 2017 *Science* **357** 294
[11] Ménard G C, Guissart S, Brun C, Leriche R T, Trif M, Debontridder F, Demaille D, Roditchev D, Simon P and Cren T 2017 *Nat. Commun.* **8** 2040
[12] Ramires A, Agterberg D F and Sigrist M 2018 *Phys. Rev.* B **98** 024501
[13] Geier M, Brouwer P W and Trifunovic L 2020 *Phys. Rev.* B **101** 245128
[14] Mackenzie A P, Scaffidi T, Hicks C W and Maeno Y 2017 *npj Quantum Mater.* **2** 40
[15] Jiao L, Howard S, Ran S, Wang Z, Rodriguez J O, Sigrist M, Wang Z, Butch N P and Madhavan V 2020 *Nature* **579** 523
[16] Fu L and Kane C L 2008 *Phys. Rev. Lett.* **100** 096407
[17] Lutchyn R M, Sau J D and Das Sarma S 2010 *Phys. Rev. Lett.* **105** 077001
[18] Oreg Y, Refael G and von Oppen F 2010 *Phys. Rev. Lett.* **105** 177002
[19] Palacio-Morales A, Mascot E, Cocklin S, Kim H, Rachel S, Morr D K and Wiesendanger R 2019 *Sci. Adv.* **5** eaav6600
[20] Trang C X *et al* 2020 *Nat. Commun.* **11** 159
[21] Escribano S D, Prada E, Oreg Y and Yeyati A L 2021 *Phys. Rev.* B **104** L041404
[22] van Loo N *et al* 2023 *Nat. Commun.* **14** 3325
[23] Prischepa S L *et al* 2021 *Supercond. Sci. Technol.* **34** 115021

[24] Kane C L and Mele E J 2005 *Phys. Rev. Lett.* **95** 146802
[25] Kane C L and Mele E J 2005 *Phys. Rev. Lett.* **95** 226801
[26] Marrazzo A, Gibertini M, Campi D, Mounet N and Marzari N 2018 *Phys. Rev. Lett.* **120** 117701
[27] Toikka L A 2019 *New J. Phys.* **21** 113033
[28] Wang Z-H, Xu F, Li L, Xu D-H, Chen W-Q, Wang B and Guo H 2021 *New J. Phys.* **23** 123002
[29] Wakatsuki R, Ezawa M and Nagaosa N 2014 *Phys. Rev.* B **89** 174514
[30] Choi W, Klein P W, Rosch A and Kim Y B 2018 *Phys. Rev.* B **98** 155123
[31] Schmidt J, Scherer D D and Black-Schaffer A M 2018 *Phys. Rev.* B **97** 014504
[32] Bernevig B A and Zhang S-C 2006 *Phys. Rev. Lett.* **96** 106802
[33] Bernevig B A, Hughes T L and Zhang S-C 2006 *Science* **314** 1757
[34] Qi X-L, Hughes T L and Zhang S-C 2010 *Phys. Rev.* B **82** 184516
[35] Meng Z Y, Lang T C, Wessel S, Assaad F F and Muramatsu A 2010 *Nature* **464** 847
[36] Hohenadler M, Lang T C and Assaad F F 2011 *Phys. Rev. Lett.* **106** 100403
[37] Zheng D, Zhang G-M and Wu C 2011 *Phys. Rev.* B **84** 205121
[38] Hohenadler M, Meng Z Y, Lang T C, Wessel S, Muramatsu A and Assaad F F 2012 *Phys. Rev.* B **85** 115132
[39] Zhou Y and Liu F 2021 *Nano Lett.* **21** 230
[40] Kitaev A Y 2006 *Ann. Phys., NY* **321** 2
[41] Cao J and Xiong S J 2013 *Phys. Rev.* B **88** 085409
[42] Sorella S and Tosatti E 1992 *Europhys. Lett.* **19** 699
[43] Manna S, Kamlapure A, Cornils L, Hänke T, Hedegaard E M J, Bremholm M, Iversen B B, Hofmann P, Wiebe J and Wiesendanger R 2017 *Nat. Commun.* **8** 14074
[44] Semenoff G W 1984 *Phys. Rev. Lett.* **53** 2449
[45] Li X, Cao T, Niu Q and Feng J 2013 *Proc. Natl Acad. Sci.* **110** 3738
[46] Xiao D, Yao W and Niu Q 2007 *Phys. Rev. Lett.* **99** 236809
[47] Zhai X and Jin G 2014 *Phys. Rev.* B **89** 235416
[48] Beenakker C W J 2006 *Phys. Rev. Lett.* **97** 067007
[49] Sau J D, Lutchyn R M, Tewari S and Das Sarma S 2010 *Phys. Rev. Lett.* **104** 040502
[50] Wang J, Zhou Q, Lian B and Zhang S-C 2015 *Phys. Rev.* B **92** 064520